Size-dependent Luminescence in HfO_2 Nanocrystals: towards White Emission from Intrinsic Surface Defects

Irene Villa[†$], *Anna Vedda*[†], *Mauro Fasoli*[†], *Roberto Lorenzi*[†], *Niklaus Kränzlin*[‡], *Felix Rechberger*[‡], *Gabriele Ilari*[▼], *Darinka Primc*[‡], *Bodo Hattendorf*[±], *Florian J. Heiligtag*[‡], *Markus Niederberger*[‡], *Alessandro Lauria*[‡*]

[†]Department of Materials Science, University of Milano-Bicocca, Via R. Cozzi 55, 20125 Milano, Italy.

[‡]Laboratory for Multifunctional Materials, Department of Materials, ETH Zürich, Vladimir-Prelog-Weg 5, 8093 Zürich, Switzerland.

[▼]Electron Microscopy Center, EMPA, Swiss Federal Laboratories for Materials Science and Technology, 8600 Dübendorf, Switzerland.

[±±] Laboratory of Inorganic Chemistry, Trace Element and Microanalysis, ETH Zürich, Vladimir-Prelog-Weg 1, 8093 Zürich, Switzerland

KEYWORDS Hafnia nanocrystals, intrinsic luminescence, rare earth free white phosphors, grain boundary, defect emission.

ABSTRACT

Defect engineering operated on metal oxides by chemical and structural modifications may strongly affect properties suitable for various applications such as photoelectrochemical behaviour, charge transport and luminescence. In this work we report the tuneable optical features observed in undoped monoclinic HfO_2 nanocrystals and their dependence on the structural properties of the material at the nanoscale. Transmission electron microscopy together with X-ray diffraction and surface area measurements were used to determine the fine structural modifications, in terms of crystal growth and coalescence of crystalline domains, occurring during a calcination process in the temperature range from 400 to 1000 °C. The fit of the broad optical emission into spectral components, together with time resolved photoluminescence, allowed us to identify the dual nature of the emission at 2.5 eV, where an ultrafast defect-related intrinsic luminescence (with decay time of few ns) overlaps with a slower emission (decay of several μs) due to extrinsic Ti - impurity centres. Moreover, the evolution of intrinsic visible bands during the material transformation was monitored. The relationship between structural parameters uniquely occurring in nanosized materials and the optical properties was investigated and tentatively modelled. The blue emissions at 2.5 and 2.9 eV are clearly related to defects lying at crystal boundaries, while an unprecedented emission at 2.1 eV enables, at relatively low calcination temperatures, the white luminescence of HfO_2 under near-UV excitation.

Introduction

Hafnium dioxide (or hafnia) is a wide band gap material denoted by outstanding physicochemical properties. It has been subject of intense research in the last twenty years mainly due to its quite high dielectric constant ($\varepsilon_r = 30$), making it a suitable alternative to silicon dioxide insulating layers for the improvement of integrated circuits.[1,2] More recently this material has been considered also as a luminescent material, due to its wide bang gap, high chemical resistance and quite high density, which makes it a good candidate host for phosphor and especially scintillator applications. In fact, the high density of the HfO_2 matrix ensures a large stopping power for ionizing radiation (X-rays, γ-rays), while the luminescence can be activated by the incorporation of elements such as rare earths (RE). Due to the restrictions of the synthesis techniques for this material, HfO_2 has been formerly studied mainly in the thin film geometry, i.e. systems confined at the nanoscale in one dimension.[3-6] Indeed the very high melting point of this oxide strongly limits the ability to produce it in the form of bulk crystal and from common crystal growth methods.[7-9] The more recent advances in colloidal preparation techniques led, in the last years, to reports concerning HfO_2 nanocrystals, where the three-dimensional confinement at the nanoscale occurs.[10-18]

The last years witnessed a growing interest of the research community on materials able to express intrinsic luminescence without the employment of RE activator impurities, which represent the current strategy for phosphor lighting,[19, 20] mainly because of the recent dramatic increase of their cost.[21-23] Intrinsic luminescence has been observed already in metal oxides like HfO_2 and ZrO_2, lying in the UV-blue region of the spectrum, that has been ascribed to the presence of point defects, such as oxygen vacancies, in the crystal lattice. [24-27] The relevance of these results lies in the opportunity to obtain new and lower cost solutions for the realization of

phosphor devices for the down-conversion of UV radiation, such as UV light emitting diodes pumped white lighting (ultraviolet-WLED).[28] Also, despite these oxides usually show luminescence excitation at relatively high energy (UVC region, $\lambda < 280$ nm),[4, 20, 24, 29] the shift of the excitation to lower energies (UVA, 315-400 nm) could be advantageous because of cheaper UV-LED as pumping sources, and might even extend their application as luminescent solar concentrators operating in the otherwise ineffective near-ultraviolet portion of the sun spectrum.[30, 31] Indeed, the optical properties of metal oxides and other classes of materials can strictly depend on peculiar structural features expressed at the nanoscale. Quantum confinement has been observed in metal oxides like Gd_2O_3 and SnO_2.[32, 33] Moreover the fine structural modifications associated with changes in NPs diameter as well as with defects concentration and ligand nature, have been proposed to be on the basis of the UV-visible tuning of the emission properties of ZnO nanostructures.[34,35] Accordingly, it is reasonable to expect that minor changes in surface elemental composition, occurrence of point defects, and lattice symmetry alterations that are typically confined at crystal interfaces, may be of major relevance in nanopowders, where a large portion of the material is actually located in close proximity to interfaces, i.e. at grain boundaries or at the crystal surface.[36-38]

In this work, we describe the occurrence of emission bands in the visible range not completely reported in literature so far, which seem to be related to the structural conformation of nanostructured crystalline HfO_2, without the employment of any dopant as luminescence activator. The dynamics of the evolution of such properties have been monitored together with the fine structural modifications, occurring in the material during the process of calcination, in the attempt to find a correlation between visible emission and both crystal size and grain boundary configuration. These phenomena govern the visible emission and excitation patterns so

enabling the tuning of the emission color depending on the annealing temperature. This approach might, in principle, represent a general strategy for the engineering of new activator-free phosphors with white emission pivoted by the structural parameters at the nanoscale.

Results and discussion

Structure and Morphology of annealed HfO_2 nanocrystals.

HfO_2 nanocrystals were synthesized by a non aqueous solvothermal method according to our previous work.[17] Shortly, Hf t-butoxide dissolved in benzyl alcohol was heated in a steel autoclave at 220 °C for 96 h. The obtained milky suspensions were thoroughly washed in diethyl ether and the precipitate was dried overnight at 60 °C. The white powder obtained by this method consists of nanoparticles (NPs) with an average diameter of 2.8 nm characterized by a slightly elongated round shape and a quite sharp size distribution. The nanocrystals are decorated by an organic layer of benzoate groups, resulting from the reaction of benzyl alcohol, which is decomposed and removed from the surface at temperatures between 400 and 500 °C [see ESI Figure S2 and S3]. For this reason the nanopowders were annealed in air at different temperatures with a heating rate of 10 °C/min and were kept for 2 h at the final temperature. From the *in situ* XRD analysis of the HfO_2 nanopowders (Figure 1a) the main structural effect of the annealing seems to be a gradual sharpening of diffraction peaks, which corresponds to increasing average crystal sizes, while the crystal geometry is monoclinic irrespective of the annealing temperature. Despite preserving a relatively small crystal size (still few tens of nm after annealing at 1000 °C, Figure S1 in the ESI) a considerable level of aggregation is observed in the TEM micrographs already for powders treated at 400 °C and above (Figure 1b-e). These complex and simultaneous phenomena of the material transformation are nevertheless associated to a significant structural modification imparted to the material. The lattice configuration is in

fact partially distorted, leading to a certain degree of disorder, which is reflected in Raman vibrational modes slightly broadened and shifted towards lower wavenumbers [Figure S4 in ESI].

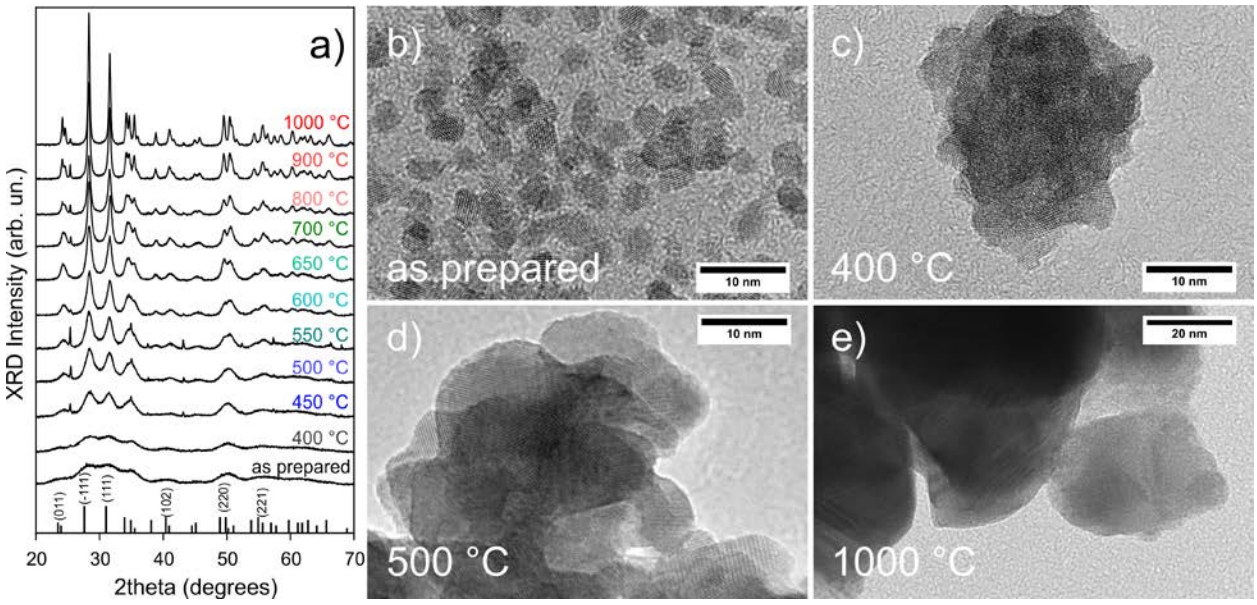

Figure 1. Structural evolution of monoclinic hafnia NPs annealed at different temperatures. In-situ XRD analysis performed on undoped HfO_2 reveals a significant crystalline domain growth starting at 450 °C (the pattern of monoclinic HfO_2 [JCPDS: 01-078-0050] is reported for reference) (a). HR-TEM micrographs of "as prepared" nanoparticles (b) and of powders annealed at 400, 500, and 1000 °C (c, d and e, respectively).

Considering the above, HfO_2 NPs can be used as a model system where, starting from crystalline ultra-small nanoparticles, only surface restructuring and lattice reconfiguration (i.e, crystal growth, sintering, and rearrangement of lattice defects) are promoted by annealing, while the monoclinic structure is kept substantially unmodified. This offers the chance to interpret the relationship between the optical properties of the material and its structure at the nanoscale, by analysing their evolution while morphological changes are imparted during calcination.

Intrinsic and Ti-related emission patterns.

Photoluminescence (PL) measurements were performed on thermally annealed undoped HfO_2 NPs. In Figure 2 some of the PL spectra obtained under 4.4 eV (280 nm) continuous wave (CW) excitation for low (Figure 2a and 2b) and high (Figure 2c) temperature treated samples are shown as a function of energy.

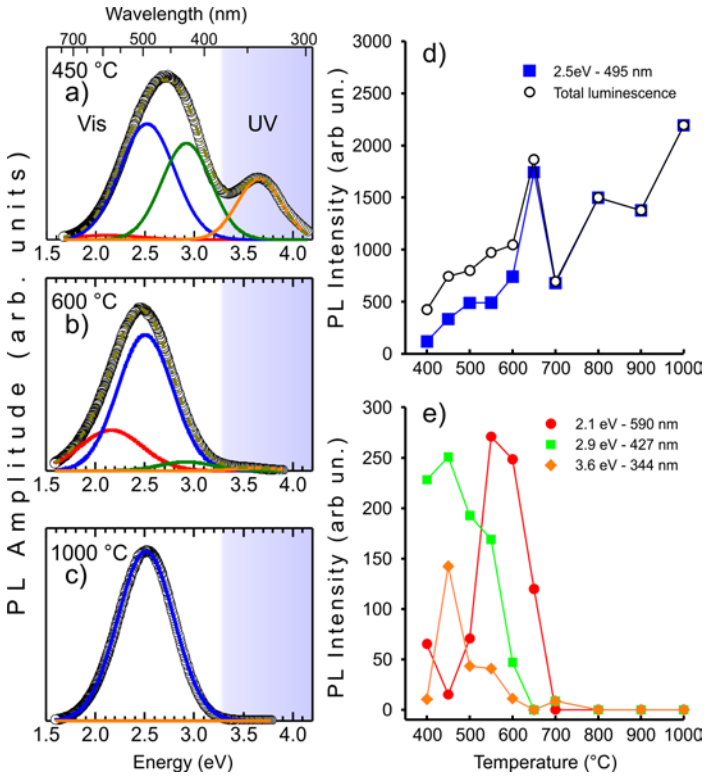

Figure 2. Dependence of the optical emissions of HfO_2 nanopowders excited at 4.4 eV (280 nm) on the annealing temperature. a), b), c): PL spectra of samples heated at 450, 600 and 1000 °C, respectively. Gaussian components (full lines) obtained by the numerical fit (green dashed line) are shown together with experimental curves (circles). d): total emission intensity (black) and intensity of the 2.5 eV component (blue) depending on the annealing temperature. e): intensity of the thermally unstable components at 2.1, 2.9 and 3.6 eV (red, green and orange, respectively). In panels d) and e) the full lines are guides for the eye.

The PL spectrum of the powder treated at 450 °C shows a broad composite emission ranging from 1.5 eV to 3.9 eV. The main effect of the annealing is the narrowing of the NPs luminescence. The intensities of all bands show clear fluctuations up to approximately 600 °C. At higher temperatures, the emission centred at 2.5 eV (490 nm), increases with temperature and dominates the PL spectrum when the sample is treated at 1000 °C; differently, the intensities of the other bands peaking at 2.1, 2.9 and 3.6 eV decrease sharply until they become barely detectable above 700 °C.

All the PL spectra were deconvolved into Gaussian components using the Levenberge - Marquardt algorithm. The fit was performed using four bands whose energy (E) and width (FWHM) values are reported in Table S3 (see ESI). Figure 2 reports the obtained deconvolution, with Gaussian fits that are in very good agreement with the experimental curves. The assignment of luminescence emissions to some specific defect centres is usually a challenging task. In the following we focus mostly on the blue emission detected in our NPs. In fact the detailed analysis of the 2.5 eV band and of its dependence upon thermal treatments allowed us to reveal some aspects of its complex nature. A blue emission in metal oxide NPs, like HfO_2 and the structurally equivalent ZrO_2, was already observed and tentatively attributed to optically active intrinsic defects and self-trapped excitons.[39, 40] Specifically, in hafnia, a band at 2.7 eV (459 nm) has been explained in terms of the presence of oxygen vacancies.[41] On the other hand, other authors suggested an extrinsic nature for a similar band observed in ZrO_2, due to the presence of some unintentional impurities like hafnium, iron, and titanium which act as primary activators.[42] Among the known different impurities in zirconia, Ti is the most probable candidate to show luminescence. The Ti^{3+} ($3d^1$) ion can be easily photoexcited and, through the radiative $3d^1$ ($e_g \rightarrow t_{2g}$) transition, it emits light at about 2.5 eV.[43] Inspired by these latter considerations, we

performed the elemental analysis on one of our samples (i.e. that annealed at 800 °C) which revealed a Ti concentration of 0.0042 ± 0.0019 at% with respect to (Hf+Zr), likely deriving from the Hf precursor.

With the aim to disclose the nature of the 2.5 eV luminescence in our HfO_2 NPs, we compared the excitation-emission features of samples calcined at increasing temperatures, with those of a sample intentionally doped with titanium (0.75 mol% nominal concentration) and treated at 1000 °C. As representative examples, in Figure 3 the photoluminescence and photoluminescence excitation (PL-PLE) spectra of undoped NPs annealed at the lowest and at the highest temperatures (400 and 1000 °C respectively) are shown, together with those of HfO_2:Ti. Relevant differences are noticed. When the undoped sample is treated at low temperature (Figure 3a), the PLE shows a dominant component at 3.5 eV (350 nm) accompanied by a shoulder at about 4.4 eV. By exciting the NPs in the dominant band at 3.5 eV, a composite spectrum is obtained displaying the 2.5 eV emission and two additional components peaking at 2.1 (590 nm) and 2.9 eV (430 nm). Their spectral positions and half-widths are similar to those of the bands obtained under 280 nm excitation (Figure 2, see also Table I and Table II of Supporting Information).

At variance, in samples treated at 1000 °C the excitation spectrum monitored at 2.5 eV emission reveals the presence of a dominant excitation component at almost 4.4 eV (Figure 3b). Moreover, the excitation at this energy leads to only one emission band at 2.5 eV. Interestingly, in this case the PL-PLE spectra are in good agreement with those of the Ti:HfO_2 sample (dot lines in Figure 3b).

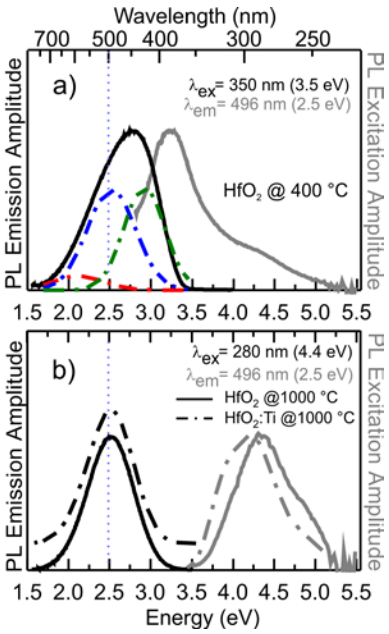

Figure 3. a): PL excitation (grey line) spectrum monitored at 2.5 eV of HfO_2 annealed at 400 °C, together with the PL emission (black lines) spectrum under 350 nm (3.54 eV) excitation. The Gaussian components of the PL spectrum are also shown (red, blue, and green dash-dot lines). The high energy side of the emission spectrum is slightly distorted by the presence of a long-pass filter, reflected on its partial mismatch with the Gaussian fit of the spectrum. b): PLE of the blue emission and PL spectra under 4.4 eV (280 nm) excitation (grey and black continuous lines, respectively) for the 1000 °C annealed NPs, compared with the Ti doped (5000 ppm) HfO_2 calcined at 1000 °C (grey and black dot lines). Vertical dot lines mark the 2.5 eV emission.

On the basis of the different excitation spectra reported in Figure 3a and 3b, a double origin of the luminescence at 2.5 eV can be suggested: i) for high annealing temperature, the emission is efficiently excited at 4.4 eV and it can be associated to a Ti-related transition; ii) at low annealing temperature, the emission is preferentially excited at lower energy, and is possibly associated to intrinsic defects of such ultra-small particles as it will be discussed later. We used time resolved photoluminescence in order to confirm the double nature of the 2.5 eV band.

Again, the fluorescence decays of annealed undoped HfO_2 NPs were also compared to that of a Ti doped HfO_2 annealed at 1000 °C. Figure 4a shows that, if the NPs are annealed at low temperature (450 °C), the PL under irradiation at 4.96 eV (250 nm) decays as a bi-exponential function with characteristic lifetimes of τ_1=1.7 ± 0.2 ns and τ_2= 7.4 ± 1.2 ns (light blue line). Moreover, the high background signal suggests the presence of a third component with a significantly longer decay time which cannot be appreciated in the nanosecond time range. This evidence has been confirmed by decay profile in the ms domain (Figure 4b) showing a triple-exponential decay with an overall half-life of 0.81 ms. Phosphorescence spectrum also suggests that the signal monitored at 2.5 eV is likely attributable to the same emission band peaking at 2.9 eV observed in steady-state measurements (see ESI, Figure S7).

After annealing at 900 °C, the PL decay changes dramatically (Figure 4c, red circles). The luminescence still decays as a bi-exponential function, but with decay times τ_1 = 1.3 ± 0.2 μs and τ_2 = 6.7 ± 0.2 μs, three order of magnitude longer with respect to the sample treated at low temperature. As a matter of fact, the observed decay is very similar to that of Ti doped hafnia NPs (Figure 4c, black circles). The dominant presence of the Ti-related transition can be explained by the reduction of non-radiative channels induced by the annealing at higher temperatures, which are expected to increase the dimension of the nanocrystals and decrease the concentration of defects (Figure 1). By excitation at 3.65 eV (340 nm) (Figure 4d), where Ti centers are poorly stimulated (Figure 3b), we observe an intrinsic blue PL emission, which shows a decay time similar to the one previously recorded for samples annealed at a lower temperature (Figure 4a). The two luminescence components of the sample annealed at 900 °C decay with lifetimes of τ_1 = 1.3 ± 0.1 ns and τ_2 = 7.7 ± 0.8 ns; in accordance with this result, the PL of the low temperature treated NPs decays as a bi-exponential function, with τ_1 = 1.4 ± 0.1 ns and τ_2 =

5.3 ± 0.5 ns. The discrepancy over the PL decay background of the two samples may be due to the presence of other luminescence components, whose emission bands overlap the 2.5 eV one and whose time decays may be longer.

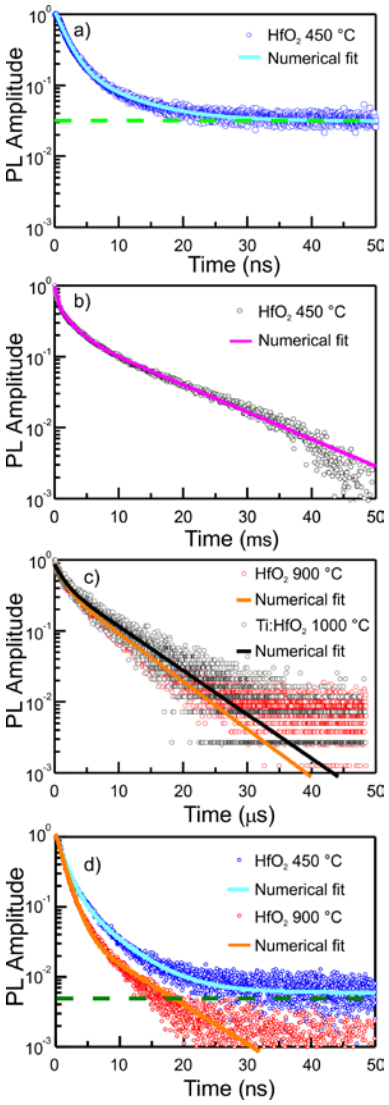

Figure 4. Time resolved photoluminescence spectra of HfO_2 annealed at different temperature under 250 nm (4.96 eV) (a, b, c) and 340 nm (3.65 eV) (d) pulsed excitation and monitoring at 490 nm (2.5 eV). Numerical fit of the decays appear as full lines.

In summary, the existence of two distinct emissions at 2.5 eV in low- and high-temperature treated samples is demonstrated by both their different excitation profiles and very different time decays.

Near-UV intrinsic fluorescence

Based on these evidences, we performed the analysis of emission spectra while exciting at lower UV energies, namely at 3.5 eV (350 nm). Nanophosphors absorbing in this energy region may be in fact also considered to be implemented in ultraviolet-WLEDs. Moreover they could be potentially suitable as downconverting materials for solar application, as the sun spectrum shows a non negligible near-UV intensity, provided that they could reach a satisfactory efficiency.[44-46] The emission spectra (Figure 5a,b,c) display the same spectral components revealed under 4.4 eV (280 nm) excitation (Figure 2). However here, in accordance with the above shown results, the band at 2.5 eV is the intrinsic fast emission and not the Ti-related one. Again, the overall shape of the spectra is clearly dependent on the annealing temperature as shown by the changes of the relative band intensities (Figure 5e). Indeed, the emission color turns from blue to cyan by increasing the temperature from 400 up to 500 °C.

After heating at 600 °C we observed a nearly white emission, with internal quantum yield (QY, i.e. number of emitted photons/number of absorbed photons) and external quantum efficiency (QE, i.e. number of emitted photons/number of incident photons) of 7.5 % and 3.1 %, respectively. While higher efficiencies of intrinsic emissions are reported for some other oxides such as ZnO and Ga_2O_3 under UVC (250 nm) excitation, no information are available on their performance in the UVA spectral region.[47,48] Significantly higher fluorescence yields in rare-earth-free oxide phosphors are reported only for systems where the near-UV excited luminescence is boosted by organic residuals or based on carbon-related defects.[28,45] For higher

temperatures we recorded a less intense blue emission (Figure 5d). The two higher energy components (violet at 2.9 eV and blue at 2.5 eV, respectively) decrease with increasing temperatures up to 700 °C (Figure 5e). The evolution of the sintering process is associated to an increase in the crystal average size (measured by the Scherrer formula applied to *ex-situ* XRD), together with the simultaneous decrease of surface specific area (obtained by Brunauer Emmett Teller (BET) gas sorption measurements). These transformations are reported in Figure 5f, and account for the rearrangement of the nanocrystals towards energy minima where the discontinuities of the lattice are reduced as long as external energy is provided to the material. The overall data displayed in Figure 5 confirm a clear dependence of the optical features upon structural parameters. More precisely, the annealing promotes the growth of crystalline domains and is reflected in a lower solid-solid interface at grain boundaries which is inversely dependent on crystal size, while the coalescence of neighbor crystallites (sintering) reflects on a lowered solid-vapor interface which was here evaluated by the measurement of specific surface area.[36]

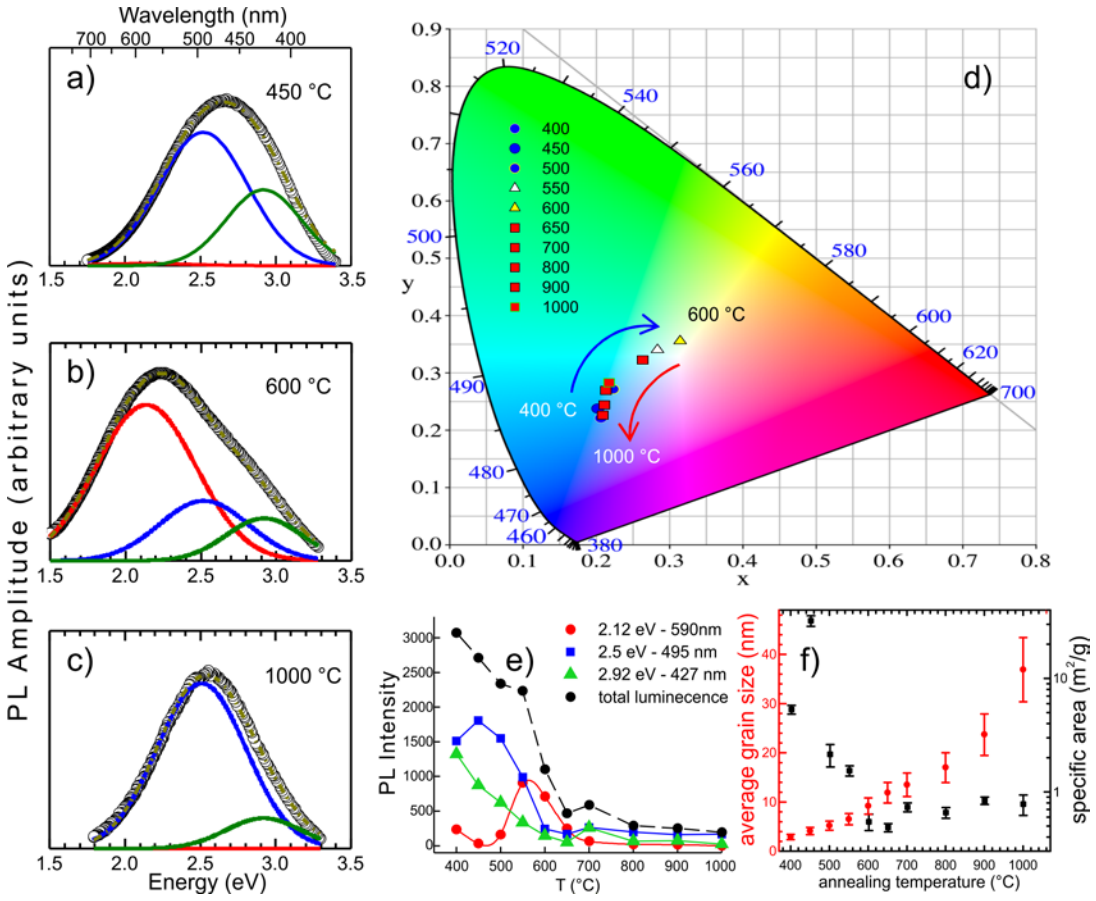

Figure 5. Evolution of visible luminescence excited at 3.5 eV (350 nm) of HfO_2 nanopowders depending on the annealing temperature. a, b, c): PL spectra of NPs treated at 450, 600 and 1000 °C, respectively. d): CIE1964 chromaticity diagram reporting the coordinates of luminescent hafnia nanopowders treated at temperatures of 400 - 500 °C (blue circles), 550 °C (white triangle), 600 °C (yellow triangle) and 650 - 1000 °C (red squares). e): absolute intensity of deconvolved components depending on annealing temperature. f): specific surface area and average crystal size recorded ex-situ on annealed samples depending on final temperature.

Correlation between intrinsic emission and structure modifications.

These measurements allowed us to suggest that different optically active defects exist in the nano-crystals, located either at inner crystal sites or at its boundaries. In a poly-crystal, the boundaries can be of two kinds: i) solid-solid interfaces between two adjacent crystallites, presenting a mismatch of the crystal lattice orientation, and ii) solid-vapor interfaces, i.e. the surface of crystal domains in contact to the environment. We tried to quantify the area of these interfaces under the approximation that crystallites are of spherical shape and constant density, leading to the total specific surface, calculated as the total area per unit mass of nanocrystals having average diameter equal to that obtained by TEM and XRD analysis. On the other hand the BET specific surface of the nanopowders was employed to directly measure the solid-vapor interface area. Despite this speculation is made under strong approximations about the material morphology, the specific grain boundaries area, i.e. the solid-solid interface, can be reasonably determined as difference between these two quantities.

In the attempt to find a correlation between the optical emissions and the structural configuration, the results of this modeling are shown in Figure 6a, where the modifications of all these three interface areas during the annealing, arising from crystal growth and sintering phenomena at increasing temperatures, are schematically sketched together with the dependence of the spectral components (excited at 350 nm where only intrinsic emissions belonging to monoclinic HfO_2 are efficiently stimulated) displayed as a function of the different interface zones. The blue components at 2.9 and 2.5 eV show a clear dependence on the material interface. Their correlation with the total grain interface, the sum of solid-solid and solid-vapor interfaces, shows, as expected, a similar yet inverse, i.e. ascending, trend with respect to temperature (Figure 5e), because of the monotonic decrease of the surface of the crystallites as their average

diameter increases during the annealing (Figure 6a). Interestingly these trends are strongly different when the bands intensities are displayed as a function of solid-solid or solid-vapor interfaces, separately.

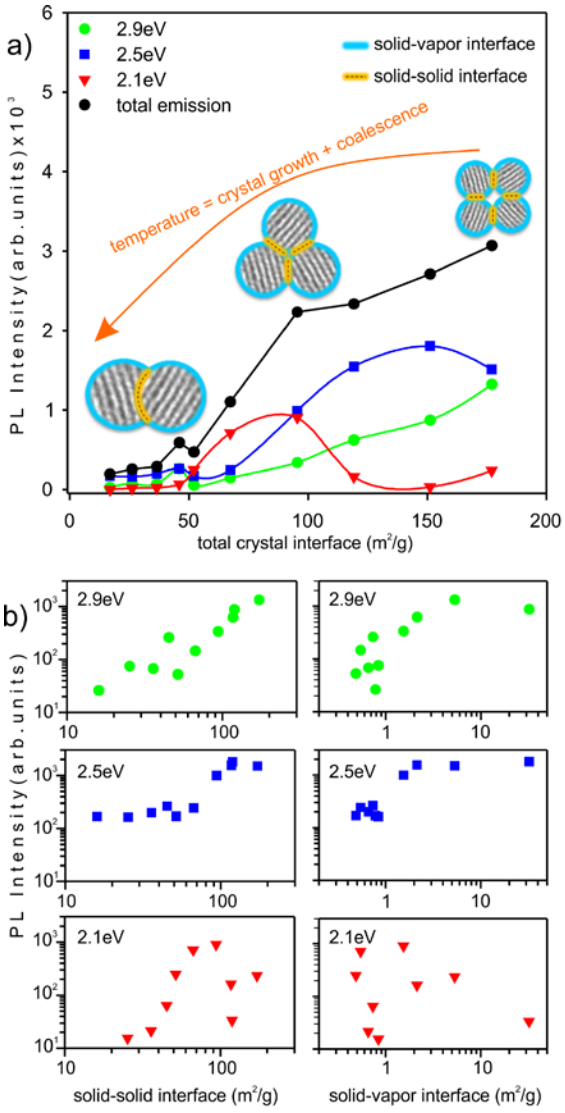

Figure 6. Dependence of the intensities of spectral components detected under 350 nm excitation on the structural parameters derived from measured crystal average size and specific surface area. a): Dependence on the total crystal interface. A representative scheme of the polycrystal structural evolution during the annealing is also shown. b): dependence of the single components either on the solid-vapor interface (measured as specific surface area by BET, right panels) or the

solid-solid interface (determined as a difference between total and solid-vapor interface, left panels).

The band at 2.9 eV shows a more clear linear dependence on the solid-solid interface, suggesting that the defect sites from which this emission originates are possibly located at the boundary between two misaligned crystallites. Inversely, its trend with respect of the solid-vapor interface manifests a *plateau* for the highest interface areas, possibly suggesting the onset of its quenching due to the interactions with species adsorbed on the outer surface of the nanocrystals. The same consideration can be done for the band at 2.5 eV, though it shows a less linear growing dependence also on the solid-solid interface. As already mentioned, oxygen vacancies can play a major role as defect centers responsible for the optical emissions at 2.9 and 2.5 eV excited in the near UV. In fact different variants of oxygen vacancies were found to be related to electronic levels in the band gap of HfO_2 by Density Functional Theory (DFT) calculations.[49,50] A link between optical emissions excited around 350 nm and oxygen vacancies was also inferred by several experimental investigations,[25,27,39] with characteristics similar to those observed for ZrO_2.[26,40] The very fast ns decay time we measured for the 2.5 eV transition is similar to the decay time values of F^+ centers in several oxides.[51-53] Nevertheless, the presence of under-coordinated ions, peculiar of nanoparticle surfaces, could also be considered as a source of optically active defects. Indeed trapping of holes by oxygen ions at the surface of HfO_2 and ZrO_2 was predicted by DFT calculations[54] while the presence of the corresponding O^- centers was revealed in ZrO_2.[55] On the other hand, a role of self-trapped excitons can be reasonably ruled out due to their expected higher excitation and emission energies.[56] The band at 2.1 eV does not show a clear dependence on any of these structural parameters, and may be more strictly related to the annealing temperature. This fact cannot be interpreted in a conclusive way, and could be

explained with a partial change in the material composition due to the incorporation of contaminants, arising from the decomposed organic capping, and which are removed or passivated for the highest annealing temperatures.[45] Alternatively, it could also arise from interface defects which are passivated, at temperatures below 500 °C, by the interaction with species coordinated to the surface, and successively reduced by the lowering of boundaries above 650 °C. Despite the nature of this latter band is still unclear, it is worth noticing that, at temperatures between 500 and 650 °C, its occurrence is responsible for the white emission of the material, representing more than 50 % of the total emission (see for reference Figure S9 in ESI).

Conclusions

In conclusion, due to the quite high strength of Hf-O bonds, the structural transformations occurring during the annealing of HfO_2 nanoparticles with very small initial diameter are relatively limited. This enabled the continuous monitoring of the evolution of all the structural transformations (organic capping decomposition, crystal growth, and coalescence) through *ex situ* investigations of the material. The contemporary analysis of the optical properties of the nanocrystals was correlated to the finely changed structural conformation occurring at the nanoscale. Such transformations impact the nanoparticle morphology revealing a rich dynamics of the emission spectral features depending on nanoscale structural characteristics of the material. It was possible to distinguish the double nature of the 2.5 eV band. At this wavelength in fact we reported the emission (best excited at 4.4 eV - 280 nm) arising from extraneous impurities of Ti^{3+} ions, denoted by slow decays in the range of microseconds. As expected, this emission dominates the spectrum after treatment at high temperature, its efficiency being gradually optimized thanks to the rearrangement of the host matrix. Emitting at the same wavelength, we recognized another optically active center (best excited in the near-UV region at

3.5 eV - 350 nm), likely of defective nature, with ultrafast decays in the range of nanoseconds. Its intensity decreases with the annealing, likely due to the thermally driven reduction of lattice defects concentration. The material exhibited a tunable luminescence under near-UV 350 nm excitation, depending on the structural configuration at the nanoscale, and not correlated to Ti impurities. Indeed, the total light output is decreased as the crystalline grade of the material increases, suggesting the defect-related nature of these optically active centers. On the one hand, blue and violet components (at 2.5 and 2.9 eV) show a clear dependence on the interfaces area and could be presumably associated to defects at crystal boundaries. On the other hand, the emission at 2.1 eV becomes dominant (explaining more than 50% of the total luminescence) only in a transitory configuration during the material transformation/sintering, being responsible for the white light emission, though showing no clear dependence on the crystal interface configuration in the material. Whatever the nature of this latter band, these results highlight the occurrence of optical features, able to dramatically enrich the emission in the visible range, that depend merely on the peculiar structural features expressed by materials confined at the nanoscale. Despite this function/structure relationship needs to be further studied, it could be of a general value and applicable also to other nanostructured metal oxides, for which defect engineering is believed to govern basic phenomena suitable for various applications from photocatalysis to microelectronics.[57,58] At the same time, the optical modifications here reported may represent a key factor for basic research on nanomaterials and drive future design strategies for luminescent dopant-free systems.

ASSOCIATED CONTENT

Supporting Information. This material is available free of charge via the Internet at http://pubs.acs.org."

AUTHOR INFORMATION

Corresponding Author

*alessandro.lauria@mat.ethz.ch

Present Addresses

$ I.V.: Departamento de Física de Materiales, Universidad Autónoma de Madrid, Ciudad Universitaria de Cantoblanco - C/Francisco Tomás y Valiente, 7 - 28049 - Madrid (Spain).

Author Contributions

The manuscript was written through contributions of all authors. All authors have given approval to the final version of the manuscript.

Funding Sources

A.L., N.K., G.I., D.P., F.R., B.H., F.H., and M.N. are grateful to ETH Zurich for financial support. R.L. acknowledges the financial support of CARIPLO Foundation under project 2012-0920.

ACKNOWLEDGMENT

The authors are grateful to E. Zych and P. Dorenbos for inspiring discussions.

REFERENCES

1. Robertson, J., High dielectric constant gate oxides for metal oxide Si transistors. *Rep. Prog. Phys.* **2006,** *69* (2), 327-396.

2. Wilk, G. D.; Wallace, R. M.; Anthony, J. M., High-kappa gate dielectrics: Current status and materials properties considerations. *J. Appl. Phys.* **2001,** *89* (10), 5243-5275.

3. Cheynet, M. C.; Pokrant, S.; Tichelaar, F. D.; Rouviere, J. L., Crystal structure and band gap determination of HfO_2 thin films. *J. Appl. Phys.* **2007,** *101* (5), 054101.

4. Kirm, M.; Aarik, J.; Jürgens, M.; Sildos, I., Thin films of HfO_2 and ZrO_2 as potential scintillators. *Nuclear Instruments and Methods in Physics Research Section A: Accelerators, Spectrometers, Detectors and Associated Equipment* **2005,** *537* (1–2), 251-255.

5. Lange, S.; Kiisk, V.; Aarik, J.; Kirm, M.; Sildos, I., Luminescence of ZrO_2 and HfO_2 thin films implanted with Eu and Er ions. *Physica status solidi (c)* **2007,** *4* (3), 938-941.

6. Lange, S.; Kiisk, V.; Reedo, V.; Kirm, M.; Aarik, J.; Sildos, I., Luminescence of RE-ions in HfO_2 thin films and some possible applications. *Opt. Mater.* **2006,** *28* (11), 1238-1242.

7. Cardarelli, F., *Material Handbook: A concise desktop references*. 2nd ed.; Springer Verlag: New York, 2008.

8. Chaubey, G. S.; Yao, Y.; Makongo, J. P. A.; Sahoo, P.; Misra, D.; Poudeu, P. F. P.; Wiley, J. B., Microstructural and thermal investigations of HfO_2 nanoparticles. *RSC Adv.* **2012,** *2* (24), 9207-9213.

9. Wang, J.; Li, H. P.; Stevens, R., Hafnia and hafnia-toughened ceramics. *J. Mater. Sci.* **1992,** *27* (20), 5397-5430.

10. Chiappini, A.; Chiasera, A.; Berneschi, S.; Armellini, C.; Carpentiero, A.; Mazzola, M.; Moser, E.; Varas, S.; Righini, G. C.; Ferrari, M., Sol-gel-derived photonic structures: Fabrication, assessment, and application. *J. Sol-Gel Sci. Technol.* **2011,** *60* (3), 408-425.

11. Buha, J.; Arcon, D.; Niederberger, M.; Djerdj, I., Solvothermal and surfactant-free synthesis of crystalline Nb_2O_5, Ta_2O_5, HfO_2, and Co-doped HfO_2 nanoparticles. *Phys. Chem. Chem. Phys.* **2010,** *12* (47), 15537-15543.

12. LeLuyer, C.; Villanueva-Ibañez, M.; Pillonnet, A.; Dujardin, C., HfO_2:X (X = Eu^{3+}, Ce^{3+}, Y^{3+}) Sol Gel Powders for Ultradense Scintillating Materials. *J. Phys. Chem. A* **2008,** *112* (41), 10152-10155.

13. Meng, J.; Jiang, D.; Li, Q., Luminescent properties of Eu^{3+}-doped HfO_2 powders prepared by combustion. *Key Eng. Mater.* **2010,** *434-435*, 805-807.

14. Wiatrowska, A.; Zych, E.; Kępiński, L., Monoclinic HfO_2:Eu X-ray phosphor. *Rad. Meas.* **2010,** *45* (3–6), 493-496.

15. Taniguchi, T.; Sakamoto, N.; Watanabe, T.; Matsushita, N.; Yoshimura, M., Rational Hydrothermal Route to Monodisperse $Hf_{1-x}Eu_xO_{2-x/2}$ Solid Solution Nanocrystals. *J. Phys. Chem. C* **2008,** *112* (13), 4884-4891.

16. Pinna, N.; Garnweitner, G.; Antonietti, M.; Niederberger, M., Non-Aqueous Synthesis of High-Purity Metal Oxide Nanopowders Using an Ether Elimination Process. *Adv. Mater.* **2004,** *16* (23-24), 2196-2200.

17. Lauria, A.; Villa, I.; Fasoli, M.; Niederberger, M.; Vedda, A., Multifunctional Role of Rare Earth Doping in Optical Materials: Nonaqueous Sol–Gel Synthesis of Stabilized Cubic HfO_2 Luminescent Nanoparticles. *ACS Nano* **2013,** *7* (8), 7041-7052.

18. De Roo, J.; De Keukeleere, K.; Feys, J.; Lommens, P.; Hens, Z.; Van Driessche, I., Fast, microwave-assisted synthesis of monodisperse HfO_2 nanoparticles. *J. Nanopart. Res.* **2013,** *15* (7), 1-11.

19. George, N. C.; Denault, K. A.; Seshadri, R., Phosphors for Solid-State White Lighting. *Annu. Rev. Mater. Res.* **2013,** *43* (1), 481-501.

20. Martínez-Martínez, R.; Álvarez, E.; Speghini, A.; Falcony, C.; Caldiño, U., Cold white light generation from hafnium oxide films activated with Ce^{3+}, Tb^{3+}, and Mn^{2+} ions. *J. Mater. Res.* **2010,** *25* (03), 484-490.

21. Lim, J. H.; Kim, B. N.; Kim, Y.; Kang, S.; Xie, R. J.; Chong, I. S.; Morita, K.; Yoshida, H.; Hiraga, K., Non-rare earth white emission phosphor: Ti-doped $MgAl_2O_4$. *Appl. Phys. Lett.* **2013,** *102* (3), 031104(1-4).

22. Ye, S.; Xiao, F.; Pan, Y. X.; Ma, Y. Y.; Zhang, Q. Y., Phosphors in phosphor-converted white light-emitting diodes: Recent advances in materials, techniques and properties. *Mater. Sci. Eng.,R* **2010,** *71* (1), 1-34.

23. Zhang, X.; Liu, W.; Wei, G. Z.; Banerjee, D.; Hu, Z.; Li, J., Systematic Approach in Designing Rare-Earth-Free Hybrid Semiconductor Phosphors for General Lighting Applications. *J. Am. Chem. Soc.* **2014,** *136* (40), 14230-14236.

24. Kiisk, V.; Lange, S.; Utt, K.; Tatte, T.; Mandar, H.; Sildos, I., Photoluminescence of sol-gel-prepared hafnia. *Physica B* **2010,** *405* (2), 758-762.

25. Wen, R.-T.; Wang, L.-S.; Guo, H.-Z.; Chen, Y.; Yue, G.-H.; Peng, D.-L.; Hihara, T.; Sumiyama, K., Blue-luminescent hafnia nanoclusters synthesized by plasma gas-phase method. *Mater. Chem. Phys.* **2011,** *130* (3), 823-826.

26. Smits, K.; Grigorjeva, L.; Millers, D.; Sarakovskis, A.; Grabis, J.; Lojkowski, W., Intrinsic defect related luminescence in ZrO_2. *J. Lumin.* **2011,** *131* (10), 2058-2062.

27. Chuang, S.-H.; Lin, H.-C.; Chen, C.-H., Oxygen vacancy relationship to photoluminescence and heat treatment methods in hafnium oxide powders. *J. Alloys Compd.* **2012,** *534*, 42-46.

28. Bai, X.; Caputo, G.; Hao, Z.; Freitas, V. T.; Zhang, J.; Longo, R. L.; Malta, O. L.; Ferreira, R. A. S.; Pinna, N., Efficient and tuneable photoluminescent boehmite hybrid nanoplates lacking metal activator centres for single-phase white LEDs. *Nat. Commun.* **2014,** *5*.

29. Aarik, J.; Mändar, H.; Kirm, M.; Pung, L., Optical characterization of HfO_2 thin films grown by atomic layer deposition. *Thin Solid Films* **2004,** *466* (1–2), 41-47.

30. McKittrick, J.; Shea-Rohwer, L. E., Review: Down Conversion Materials for Solid-State Lighting. *J. Am. Ceram. Soc.* **2014,** *97* (5), 1327-1352.

31. Huang, X., Solid-state lighting: Red phosphor converts white LEDs. *Nat. Photon.* **2014,** *8* (10), 748-749.

32. Mercier, B.; Ledoux, G.; Dujardin, C.; Nicolas, D.; Masenelli, B.; Melinon, P.; Bergeret, G., Quantum confinement effect on Gd_2O_3 clusters. *J. Chem. Phys.* **2007,** *126* (4), 044507-7.

33. Lee, E. J. H.; Ribeiro, C.; Giraldi, T. R.; Longo, E.; Leite, E. R.; Varela, J. A., Photoluminescence in quantum-confined SnO_2 nanocrystals: Evidence of free exciton decay. *Appl. Phys. Lett.* **2004,** *84* (10), 1745-1747.

34. Hsu, H. C.; Huang, H. Y.; Eriksson, M. O.; Dai, T. F.; Holtz, P. O., Surface related and intrinsic exciton recombination dynamics in ZnO nanoparticles synthesized by a sol-gel method. *Appl. Phys. Lett.* **2013,** *102* (1), 013109(1-4).

35. Hung, C.-H.; Whang, W.-T., Effect of surface stabilization of nanoparticles on luminescent characteristics in ZnO/poly(hydroxyethyl methacrylate) nanohybrid films. *J. Mater. Chem.* **2005,** *15* (2), 267-274.

36. Castro, R. H. R.; Tôrres, R. B.; Pereira, G. J.; Gouvêa, D., Interface Energy Measurement of MgO and ZnO: Understanding the Thermodynamic Stability of Nanoparticles. *Chem. Mater.* **2010,** *22* (8), 2502-2509.

37. Foster, A. S.; Lopez Gejo, F.; Shluger, A. L.; Nieminen, R. M., Vacancy and interstitial defects in hafnia. *Phys. Rev. B* **2002,** *65* (17), 174117.

38. Wang, Z.; Saito, M.; McKenna, K. P.; Gu, L.; Tsukimoto, S.; Shluger, A. L.; Ikuhara, Y., Atom-resolved imaging of ordered defect superstructures at individual grain boundaries. *Nature* **2011,** *479* (7373), 380-383.

39. Bai, X.; Pucci, A.; Freitas, V. T.; Ferreira, R. A. S.; Pinna, N., One-Step Synthesis and Optical Properties of Benzoate- and Biphenolate-Capped ZrO_2 Nanoparticles. *Adv. Funct. Mater.* **2012,** *22* (20), 4275-4283.

40. Rauwel, E.; Galeckas, A.; Rauwel, P., Photoluminescent cubic and monoclinic HfO_2 nanoparticles: effects of temperature and ambient. *Mater. Res. Express* **2014,** *1* (1), 015035.

41. Perevalov, T. V.; Aliev, V. S.; Gritsenko, V. A.; Saraev, A. A.; Kaichev, V. V.; Ivanova, E. V.; Zamoryanskaya, M. V., The origin of 2.7 eV luminescence and 5.2 eV excitation band in hafnium oxide. *Appl. Phys. Lett.* **2014,** *104* (7), 071904(1-4).

42. Carvalho, J.; Rodrigues, L. V.; Felinto, M. F. C.; Nunes, L. O.; Hölsä, J.; Brito, H., Structure–property relationship of luminescent zirconia nanomaterials obtained by sol–gel method. *J. Mater. Sci.* **2015,** *50* (2), 873-881.

43. Fiaczyk, K.; Wojtowicz, A. J.; Zych, E., Photoluminescent Properties of Monoclinic HfO_2:Ti Sintered Ceramics in 16-300 K. *J. Phys. Chem. C* **2015,** *119*, 5026-5032.

44. Huang, X.; Han, S.; Huang, W.; Liu, X., Enhancing solar cell efficiency: the search for luminescent materials as spectral converters. *Chem. Soc. Rev.* **2013,** *42* (1), 173-201.

45. Shang, M.; Li, C.; Lin, J., How to produce white light in a single-phase host? *Chem. Soc. Rev.* **2014,** *43* (5), 1372-1386.

46. van der Ende, B. M.; Aarts, L.; Meijerink, A., Lanthanide ions as spectral converters for solar cells. *Phys. Chem. Chem. Phys.* **2009,** *11* (47), 11081-11095.

47. Wang, T.; Farvid, S. S.; Abulikemu, M.; Radovanovic, P. V., Size-Tunable Phosphorescence in Colloidal Metastable γ-Ga_2O_3 Nanocrystals. J. Am. Chem. Soc. 2010, 132, 9250-9252.

48. van Dijken, A.; Makkinje, J.; Meijerink, A., The influence of particle size on the luminescence quantum efficiency of nanocrystalline ZnO particles. J. Lumin. 2001, 92, 323-328

49. Muñoz Ramo, D.; Gavartin, J. L.; Shluger, A. L.; Bersuker, G., Spectroscopic Properties of Oxygen Vacancies in Monoclinic HfO_2 Calculated with Periodic and Embedded Cluster Density Functional Theory. *Phys. Rev. B* **2007,** *75,* 205336.

50. Broqvist, P.; Pasquarello, A., Oxygen Vacancy in Monoclinic HfO_2: A Consistent Interpretation of Trap Assisted Conduction, Direct Electron Injection, and Optical Absorption Experiments. *Appl. Phys. Lett.* **2006,** *89,* 262904.

51. Zorenko, Y.; Zorenko, T.; Voznyak, T.; Mandowski, A.; Qi, X.; Batentschuk, M.; Friedrich, J., Luminescence of F+ and F Centers in Al_2O_3 - Y_2O_3 Oxide Compounds. *IOP Conference Series: Materials Science and Engineering* **2010,** *15*, 012060.

52. Babin, V.; Laguta, V. V.; Maaroos, A.; Makhov, A.; Nikl, M.; Zazubovich, S., Luminescence of F^+-Type Centers in Undoped $Lu_3Al_5O_{12}$ Single Crystals. *Physica Status Solidi (B) Basic Research* **2011,** *248*, 239-242.

53. Rosenblatt, G. H.; Rowe, M. W.; Williams Jr, G. P.; Williams, R. T.; Chen, Y., Luminescence of F and F+ Centers in Magnesium Oxide. *Phys. Rev. B* **1989,** *39*, 10309-10318.

54. Wolf, M. J.; McKenna, K. P.; Shluger, A. L., Hole Trapping at Surfaces of M-ZrO_2 and M-HfO_2 Nanocrystals. *J. Phys. Chem. C* **2012,** *116*, 25888-25897.

55. Emeline, A. V.; Panasuk, A. V.; Sheremetyeva, N.; Serpone, N., Mechanistic Studies of the Formation of Different States of Oxygen on Irradiated ZrO_2 and the Photocatalytic Nature of

Photoprocesses from Determination of Turnover Numbers. *J. Phys. Chem. B* **2005,** *109*, 2785-2792.

56. Muñoz Ramo, D.; Sushko, P. V.; Shluger, A. L., Models of Triplet Self-Trapped Excitons in SiO_2 , HfO_2, and $HfSiO_4$. *Phys. Rev. B* **2012,** *85*, 024120.

57. Osterloh, F. E., Inorganic Nanostructures for Photoelectrochemical and Photocatalytic Water Splitting. *Chem. Soc. Rev.* **2013,** *42*, 2294-2320.

58. Seebauer, E. G.; Noh, K. W., Trends in Semiconductor Defect Engineering at the Nanoscale. *Materials Science and Engineering: R: Reports* **2010,** *70*, 151-168.

Table of Contents: